

From low-density neutron matter to the unitary limit

T. Abe¹ * and R. Seki²

¹ *Department of Physics, Tokyo Institute of Technology, Meguro, Tokyo 152-8551, Japan*

² *Department of Physics and Astronomy, California State University,
Northridge, Northridge, CA 91330, USA*

(Dated: October 22, 2018)

Abstract

Various quantities of an attractively interacting fermion system at the unitary limit are determined by extrapolating Monte Carlo results of low-density neutron matter. Smooth extrapolation in terms of $1/(k_F a_0)$ (k_F is the Fermi momentum, and a_0 is the 1S_0 scattering length) is found with the quantities examined: the ground-state energy, the pairing gap at $T \approx 0$, and the critical temperature of the normal-to-superfluid phase transition. We emphasize proximity of the physics of low-density neutron matter to that at the unitary limit. The extrapolated quantities are in a reasonable agreement with those in the literature.

PACS numbers: 21.60.Ka, 21.65.-f, 71.10.Fd, 74.20.Fg

arXiv:0708.2524v3 [nucl-th] 12 May 2009

* Current address: Center for Nuclear Study, Graduate School of Science, the University of Tokyo, RIKEN Campus, Wako, Saitama 351-0198, Japan

I. INTRODUCTION

In our previous paper [1], we reported a Monte Carlo calculation of thermodynamic properties of low-density neutron matter by using nuclear effective field theory (EFT) [2]. As pairing in neutron matter is strong, neutron matter is a strongly correlated fermionic system. We firmly established that low-density neutron matter is in the state of BCS-Bose-Einstein condensation (BEC) crossover [3] instead of a BCS-like state, the standard description in nuclear physics [4].

The crossover state of low-density neutron matter is actually an expected one from studies of the BCS-BEC crossover over the past decade. The pairing strength of an attractively interacting (therefore unstable) fermion system is characterized by a product of the two physical parameters, the Fermi momentum k_F and the (S -wave) scattering length a_0 [5]. In terms of $\eta \equiv 1/(k_F a_0)$, the state of the BCS limit is realized at $\eta \rightarrow -\infty$, that of the BEC limit at $\eta \rightarrow +\infty$, and that of the unitary limit at $\eta \rightarrow 0$. (We use the sign convention $a_0 < 0$ for fermions attractively interacting with no bound state.) A fermion pair at the limit forms a zero-energy bound state, thereby yielding an infinitely long scattering length. Because the infinitely long scattering length generates no classical scale, the fermion system composed of the pairs is expected to have a universal feature. In recent years, much attention has been paid to the physics at the unitary limit in the fields of both condensed matter and atomic physics; for example, Refs. [6, 7], and references therein. The 1S_0 neutron-neutron scattering length is negative and large in magnitude, $a_0 \approx -16.45$ fm [8]. For a density of about $(10^{-4} - 10^{-2})\rho_0$ ($\rho_0 = 0.16$ fm $^{-3}$ is the nuclear matter density), η takes the value of

$$-0.8 \lesssim \eta \lesssim -0.2. \quad (1)$$

Furthermore, the neutron matter of the above density is well described by the EFT lattice Hamiltonian that is identical to the attractive Hubbard model [9]. Equation (1) thus suggests that the physics of low-density neutron matter would be similar to that of the unitary limit. Note that the similarity is expected only in the limited range of the density. For $\eta \ll -0.8$ ($\eta \rightarrow -\infty$), neutron matter would be in more of a BCS state in this quite low density. For $\eta \gtrsim -0.2$ ($\eta \rightarrow 0$), the physics of neutron matter is much affected by the next-order (repulsive) term in the EFT potential, and deviates from that of the unitary limit.

Physically, neutron matter never reaches the unitary limit $\eta = 0$. But our previous Monte Carlo results at the leading-order (LO) [1] are based on the Hubbard model with

the parameter values chosen (translated from k_F and a_0) to be suitable for neutron matter. A Monte Carlo calculation of a fermion system at the unitary limit could be carried out by repeating our neutron-matter calculation but with the parameter values adjusted to the limit. This approach has been used by Lee [10, 11, 12, 13], based on the Lagrangian formalism. While it may appear to be a straight-forward application, the computation is quite time consuming. Instead, by exploiting the proximity of low-density neutron matter to the unitary limit, we follow here another procedure originally proposed in Ref. [14], an extrapolation to the unitary limit from low-density neutron matter by use of our previous Monte Carlo results at the LO.

The underlying assumption in this procedure is that the physical quantities of interest are, at least numerically, slowly varying functions of η and smoothly reachable to the unitary limit, as Eq. (1) suggests. As will be seen in Secs. III and IV, we find that this is indeed the case. The quantities examined are the ground-state energy $E_{g.s.}$, the pairing gap at $T \approx 0$, Δ , and the critical temperature of the normal-to-superfluid phase transition T_c , all of which are made to be dimensionless by taking ratios with $\epsilon_F \equiv k_F^2/(2M)$ (M is the neutron mass). Note that only k_F provides a classical dimension at the unitary limit in the system.

This paper is organized as follows: After the Introduction. Sec. II briefly summarizes our computational method, which will help keep the discussions in later sections coherent. In Secs. III, IV, and V, we describe the extrapolation procedure of $E_{g.s.}$, Δ , and T_c , respectively. The description of $E_{g.s.}$ in Sec. III is somewhat detailed, since this quantity was not examined in our previous paper [1]. Our conclusion is found in Sec. VI.

II. MONTE CARLO COMPUTATION FOR THE STANDARD PARAMETER SET

The neutron-neutron (nn) interaction in the EFT Lagrangian includes all possible terms allowed by symmetries of the underlying theory of quantum chromodynamics (QCD) [2]. The nn potential is in the momentum expansion form

$$V(\mathbf{p}', \mathbf{p}) = c_0(\Lambda) + c_2(\Lambda)(\mathbf{p}^2 + \mathbf{p}'^2) + \dots - 2c_2(\Lambda)\mathbf{p} \cdot \mathbf{p}' + \dots, \quad (2)$$

where \mathbf{p} and \mathbf{p}' are the nn center-of-mass momenta, and Λ is the regularization scale. For a description of low-density neutron matter, we use a truncated potential including only the

first term in Eq. (2). The truncated EFT Hamiltonian on a three-dimensional cubic lattice \hat{H} then takes the form of the three-dimensional attractive Hubbard-model Hamiltonian [9],

$$\begin{aligned}\hat{H} &= -t \sum_{\langle i,j \rangle \sigma} \hat{c}_{i\sigma}^\dagger \hat{c}_{j\sigma} + 6t \sum_{i\sigma} \hat{c}_{i\sigma}^\dagger \hat{c}_{i\sigma} + \frac{1}{a^3} c_0(a) \sum_i \hat{c}_{i\uparrow}^\dagger \hat{c}_{i\downarrow}^\dagger \hat{c}_{i\downarrow} \hat{c}_{i\uparrow} \\ &= -t \sum_{\langle i,j \rangle \sigma} \hat{c}_{i\sigma}^\dagger \hat{c}_{j\sigma} + 6t \sum_{i\sigma} \hat{n}_{i\sigma} + \frac{1}{a^3} c_0(a) \sum_i \hat{n}_{i\uparrow} \hat{n}_{i\downarrow},\end{aligned}\quad (3)$$

where a is the lattice spacing, $t = 1/(2Ma^2)$ is the hopping parameter (M , the neutron mass), and $\langle i, j \rangle$ denotes a restriction on the sum of all neighboring pairs. $\hat{c}_{i\sigma}^\dagger$ and $\hat{c}_{i\sigma}$ are the creation and annihilation operators of the neutron, respectively ($\sigma = \uparrow, \downarrow$), and $\hat{n}_{i\sigma} = \hat{c}_{i\sigma}^\dagger \hat{c}_{i\sigma}$ is the number operator with the spin σ at the i site.

The lattice spacing a is directly related to Λ as

$$\Lambda \sim \frac{\pi}{a}. \quad (4)$$

Λ should be set larger than the momentum scale, below which the truncated form of the potential is valid [15]. Λ can be chosen to be smaller but should be at least

$$\Lambda > p \quad (5)$$

for the momentum p at which the physics is studied [16]. In our case, we take $p \sim k_F$, because the momentum scale corresponding to the excitation energy of interest is much less.

The EFT parameter $c_0(a)$ in the lattice regularization with the finite lattice spacing a is given as [17]

$$c_0(a) = \frac{4\pi}{M} \left(\frac{1}{a_0} - \frac{2\theta_1}{a} \right)^{-1}, \quad (6)$$

where

$$\theta_1 \equiv \frac{1}{8\pi^2} \wp \int_{-\pi}^{\pi} \int_{-\pi}^{\pi} \int_{-\pi}^{\pi} \frac{dx dy dz}{3 - (\cos x + \cos y + \cos z)} = 1.58796 \dots \quad (7)$$

is a form of Watson's triple integral [18], with \wp denoting the principal value of the integral. At the unitary limit ($|a_0| \rightarrow \infty$), we have

$$c_0(a)/(a^3 t) \rightarrow -4\pi/\theta_1 = -7.91353 \dots, \quad (8)$$

which agrees with the value found in the literature [6].

In our Monte Carlo calculation at the LO [1], we carried out an extensive Monte Carlo lattice calculation for the standard parameter set, which consists of the three values of the

neutron matter density ρ with the lattice filling (or the site-occupation fraction) n set to be $1/4$. The reasoning underlying this choice is somewhat involved, and we refer the reader to our previous paper [1]. Here, n is defined as

$$n \equiv a^3 \rho = \frac{1}{N_s} \sum_{i,\sigma} \langle \hat{c}_{i\sigma}^\dagger \hat{c}_{i\sigma} \rangle, \quad (9)$$

where N_s is the lattice size (the total number of the three-dimensional lattice sites). Note that in this work, we specify the density of the interacting fermion system, ρ , using k_F through the relation $\rho = k_F^3/(3\pi^2)$. We emphasize that ρ here is an expectation value obtained by our Monte Carlo calculation, as Eq. (9) shows.

The three densities of the standard parameter set are $k_F = 15, 30, \text{ and } 60$ MeV. The corresponding three values of η are listed in Table I, together with those of a and $c_0(a)$, which follow from the k_F values with $n = 1/4$. Though not used in the Monte Carlo calculation, the value of $c_0(a)$ at the unitary limit, Eq. (8), is also shown in the table for comparison. Note that a in the standard parameter set satisfies the EFT regularization condition, Eq. (5).

TABLE I: Standard parameter set and $c_0(a)/(a^3 t)$ at the unitary limit $\eta = 0$.

η	$c_0/(a^3 t)$	k_F (MeV)	a (fm)	Λ (MeV)
-0.7997	-5.308	15	25.64	24.18
-0.3999	-6.354	30	12.82	48.36
-0.1999	-7.049	60	6.409	96.73
0.0000	-7.914			

The Monte Carlo calculations were performed on cubic lattices of $N_s = 4^3, 6^3, 8^3, \text{ and } 10^3$ by the method of determinantal quantum Monte Carlo [19, 20], commonly used in condensed-matter physics. Using the data on the four different N_s 's, we apply the method of finite-size scaling to extrapolate to the thermodynamic limit. We take the continuum limit ($n \rightarrow 0$) by extrapolation using Monte Carlo data for various n 's on the $N_s = 6^3$ lattice. In the following section we elaborate on how we determine $E_{g.s.}$ at these limits and how we then extrapolate to $\eta \rightarrow 0$.

III. GROUND-STATE ENERGY $E_{g.s.}$

Following common practice, we express the ground-state energy per particle of neutron matter $E_{g.s.}$ in terms of the energy parameter ξ ,

$$\xi = \frac{E_{g.s.}}{E_{FG}} = \frac{5E_{g.s.}}{3\epsilon_F}, \quad (10)$$

where E_{FG} is the ground-state energy per particle of the corresponding noninteracting system. ξ is expected to be of a universal character at the unitary limit. As done in our previous paper, we determine ξ at the three values of η from the LO lattice calculations, first by taking the thermodynamic limit and second by applying the continuum limit. After carrying out the two steps, we extrapolate ξ to $\eta = 0$.

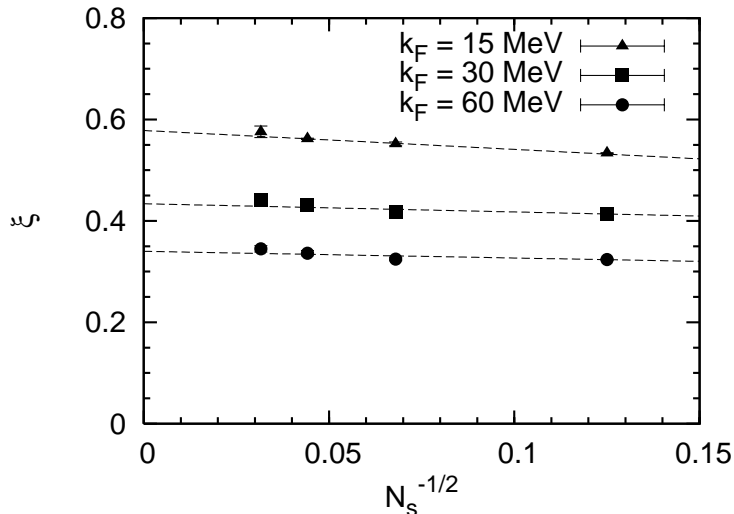


FIG. 1: Finite-size scaling of the energy parameter ξ . The thermodynamic limit is at $N_s \rightarrow \infty$. The Monte Carlo data of ξ with statistical uncertainties are shown at the Fermi momentum of $k_F = 15$ (triangle), 30 (square), and 60 MeV (circle). The dotted lines are the $N_s^{-1/2}$ linear fits, Eq. (11), to the data of $N_s = 4^3, 6^3, 8^3$, and 10^3 .

First, we determine ξ of the thermodynamic limit at the three η by applying the method of finite-size scaling using Monte Carlo data for the four lattice sizes, $N_s = 4^3, 6^3, 8^3$, and 10^3 . The data used for the determination are shown with statistical uncertainties in Fig. 1.

As in the case of Δ discussed in Ref. [1], the N_s dependence of ξ is found to be weak. The scaling exponent is difficult to determine, and the best fit to the Monte Carlo data results

in an exponent with a large uncertainty, essentially being indefinite. As shown in Fig. 1, we find the choice of the N_s scaling power of ξ , $\sim N_s^{-1/2}$ (the same as that of Δ [1]) works reasonably well though not quite ideally. Because of the limited number of our Monte Carlo data, we decided to proceed with the analysis using the $N_s^{-1/2}$ scaling. With this scaling, the best fits are found to be

$$\begin{aligned}\xi(\eta \approx -0.8, N_s) &= -0.37(13) N_s^{-1/2} + 0.5784(35), \\ \xi(\eta \approx -0.4, N_s) &= -0.162(84) N_s^{-1/2} + 0.4339(75), \\ \xi(\eta \approx -0.2, N_s) &= -0.131(63) N_s^{-1/2} + 0.3400(80),\end{aligned}\tag{11}$$

and are shown with the Monte Carlo data in Fig. 1. The last constant in each equation in Eq. (11) is ξ in the thermodynamic limit ($N_s \rightarrow \infty$).

The preceding best fits are performed using the jackknife method (often used in the lattice QCD data analysis [21]). The method is used to obtain all best fits in this work.

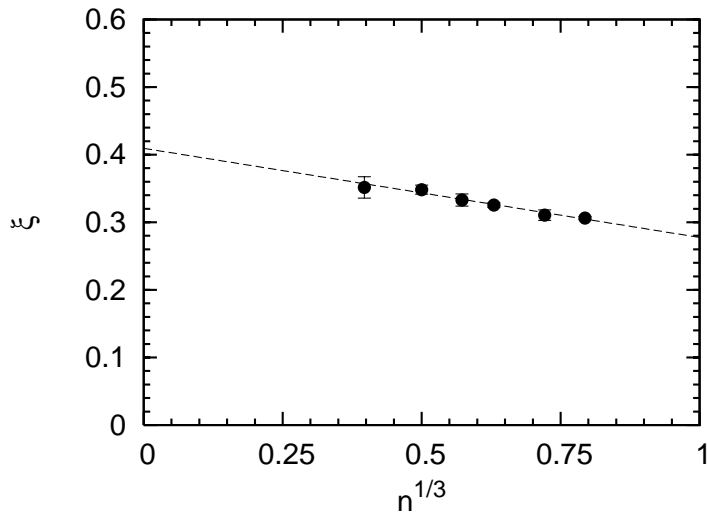


FIG. 2: Energy parameter ξ as a function of the lattice filling n . Monte Carlo data (solid circles with statistical uncertainties) are for $n = 1/16, 1/8, 3/16, 1/4, 3/8,$ and $1/2$ on the $N_s = 6^3$ lattice for $k_F = 60$ MeV. The dashed line, Eq. (12), is the best fit to the data.

Second, we take the continuum limit through $n \rightarrow 0$ in a procedure similar to that in Ref. [6], as discussed in Ref. [1]. As shown in Fig. 2, the Monte Carlo data for the lattice fillings of $n = 1/16, 1/8, 3/16, 1/4, 3/8,$ and $1/2$ are best fit by

$$\xi(n) = -0.132(24) n^{1/3} + 0.409(15).\tag{12}$$

Note that $n = 1/2$ corresponds to the quarter filling of the lattice. The data are taken on a lattice of $N_s = 6^3$ at the Fermi momentum $k_F = 60$ MeV. Equation (12) gives the ratio of $\xi(n \rightarrow 0)$ and $\xi(n = 1/4)$ as 1.26(6).

As discussed in Ref. [1], such a ratio is expected and is also confirmed to depend weakly on N_s and k_F in the case of Δ at $T \approx 0$, T_c , and the pairing temperature scale T^* . Here, we assume that ξ also weakly depends on N_s and k_F . Applying the same ratio to ξ at the thermodynamic limit, we then obtain

$$\begin{aligned}\xi(\eta \approx -0.8) &= 0.728(37), \\ \xi(\eta \approx -0.4) &= 0.546(34), \\ \xi(\eta \approx -0.2) &= 0.428(30).\end{aligned}\tag{13}$$

The three values of ξ of Eq. (13) are best fitted by

$$\xi = 0.292(24) - 0.795(33) \eta - 0.271(21) \eta^2,\tag{14}$$

which yields $\xi = 0.292(24)$ at the unitary limit by setting $\eta \rightarrow 0$. Note that Eq. (14) is similar to $\xi = 0.306(1) - 0.805(2)\eta - 0.63(3)\eta^2$ in Ref. [22] and gives $d\xi/d\eta|_{\eta=0} = -0.795(33)$ close to $-1.0(1)$ in Ref. [10].

Figure 3 shows the three ξ values of Eq. (13) and their best fit Eq. (14), together with ξ at the unitary limit. In the figure, we also show several results of the η dependence of ξ reported in the literature. They include the two types of calculations: (i) analytical and (ii) numerical.

(i) This type is an ϵ -expansion calculation at the next-to-leading order (NLO) [23] about four dimension (shown by the dash-dotted curve). Note that a recent next-to-next-to-leading order (NNLO) calculation at $\eta = 0$ [24] shows the appearance of a problematic $\ln \epsilon$ contribution, but it is argued to be infrared manageable.

(ii) The Monte Carlo types of calculation include the lattice Monte Carlo calculation with the symmetric heavy-light ansatz [22] (shown by the dotted curve), the diffusion Monte Carlo method [25] (cross symbols), the fixed-node Green's function Monte Carlo method at $\eta < 0$ (solid up-triangles) [26], and at $\eta = 0$ (solid down-triangle) [27], and the determinantal quantum Monte Carlo method (solid squares) [28, 29]. Note that the previously reported ξ by the fixed-node Green's function Monte Carlo calculations [30, 31] (solid diamonds) were

somewhat larger, being near that of Ref. [25]. We further note that no thermodynamic limit is taken in these Monte Carlo calculations.

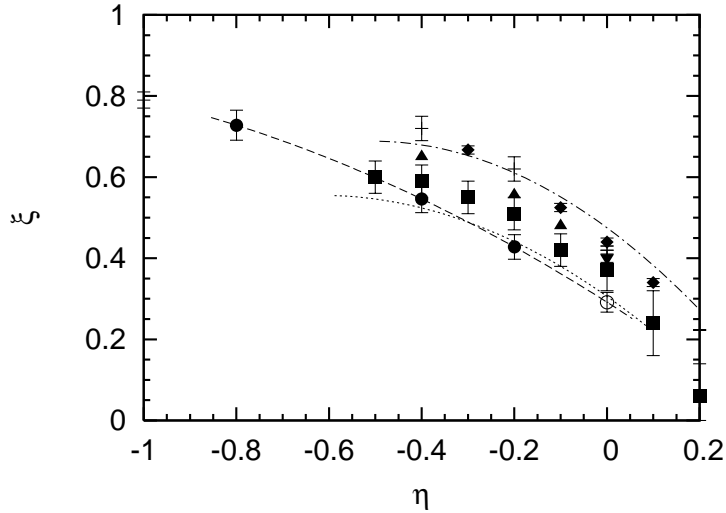


FIG. 3: $\eta \equiv 1/(k_F a_0)$ dependence of the energy parameter ξ . The solid circles and the dashed curve are our Monte Carlo data and the best-fit, Eq. (14), respectively. Our ξ extrapolated to the unitary limit is shown by the open circle. For comparison, ξ obtained by other works are also shown: the dash-dotted curve is by the next-to-leading order ϵ expansion [23], the dotted curve is by the lattice Monte Carlo calculation with the symmetric heavy-light ansatz [22], the cross symbols are by the fixed-node diffusion Monte Carlo calculation [25], the solid up- and down-triangles are by the fixed-node Green's function Monte Carlo calculations at $\eta < 0$ [26] and at $\eta = 0$ [27], respectively, and the solid squares are by the determinantal quantum Monte Carlo calculation [28, 29].

In Fig. 4, we compare our result with various values of the unitary-limit ξ in the literature. The figure is made by expanding a similar figure (Fig. 14) in Ref. [24]. On the left-hand side of the figure, the values of ξ determined by atomic Fermi-gas experiments are shown by solid circles: $\xi = 0.74(7)$ [32], $\xi = 0.34(15)$ [33], $\xi = 0.32^{+0.13}_{-0.10}$ [34], $\xi = 0.46(5)$ [35], and $\xi = 0.51(4)$ [36].

In the middle of Fig. 4, the values of ξ obtained by various Monte Carlo calculations are shown by the solid squares: $\xi \leq 0.42(1)$ [27], $\xi = 0.25(3)$ [10], $0.07 \leq \xi \leq 0.42$ [11], $\xi \approx 0.44$ [37], $\xi \approx 0.28$ [22], $\xi = 0.292(12)$ and $0.329(5)$ [12], and $\xi = 0.37(5)$ [28, 29]. For comparison, our result, Eq. (14), is shown by the diamond.

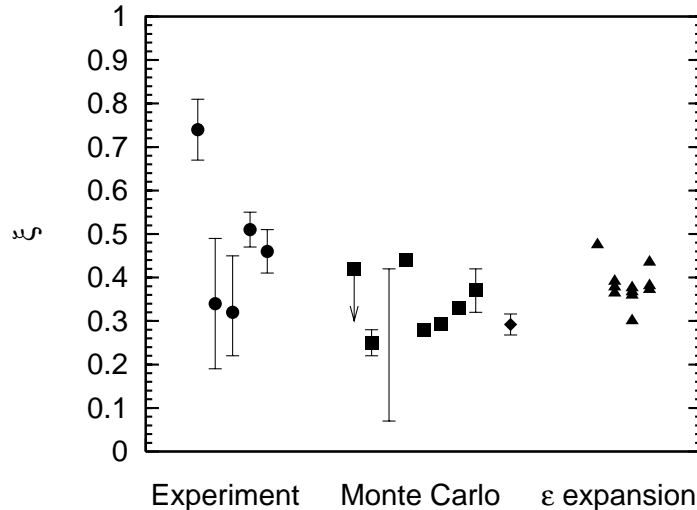


FIG. 4: ξ at the unitary limit. The values of ξ reported in the literature are shown in three groups from left to right: those determined by atomic Fermi-gas experiments (solid circles); by various Monte Carlo calculations (solid squares); and by ϵ expansions (triangles). The scale of the horizontal axis has no significance but for separating data. ξ 's by the ϵ -expansion method on the right-hand side are divided into three subgroups as explained in the text. Our ξ from Eq. (14) is shown by the diamond at the right-most location in the Monte Carlo group. See the text for the reference to each value of ξ . The figure is an expanded version of a similar figure (Fig. 14) in Ref. [24].

On the right-hand side of the figure, the values of ξ by the ϵ expansions are shown by triangles in three groups: from left to right, (1) the NLO ϵ expansion [38], (2) the Borel-Padé approximation between the NLO expansions about four and two dimensions [39], (3) the Borel-Padé approximation between the NNLO expansion around four dimensions and the NLO expansion about two dimensions [24], and (4) the Borel-Padé approximation between the NNLO expansions about four and two dimensions [40].

Figure 4 shows that our value of ξ , 0.292(24), is relatively small among the values shown.

IV. PAIRING GAP Δ

The pairing gap Δ at the unitary limit may be simply related to $E_{g.s.}$ as $\sim 2E_{g.s.}$ [30]. To examine the relationship, we determined Δ for $\eta \rightarrow 0$ by extrapolation.

In Fig. 5, we show Δ in the thermodynamic and continuum limits for the three values of η by taking from our previous work at the LO [1]. The figure also shows the best-fit curve to the three η values using the quadratic function

$$\frac{\Delta}{\epsilon_F} = 0.384(30) + 0.303(27) \eta + 0.046(37) \eta^2, \quad (15)$$

from which $\Delta/\epsilon_F = 0.384(30)$ is determined by setting $\eta = 0$. The figure includes other quantum Monte Carlo results: the solid squares are by Bulgac *et al.* [28, 29], the solid up-triangles are by Gezerlis *et al.* [26], the solid down-triangle is by Carlson *et al.* [27], and the solid diamonds are by Chang *et al.* [31]. Figure 5 is drawn similar to Fig. 1 of Ref. [28] and to Fig. 14 of Ref. [29]. Note that the data by Chang *et al.* at $\eta < 0$ are those quoted in Refs. [28, 29].

The relation between Δ and $E_{g.s.}$ is found from that of Δ and η by eliminating ϵ_F from Eqs. (10) and (15) and by using ξ of Eq. (14) at $\eta = 0$. Table II summarizes our result. Our $\Delta/E_{g.s.}$ at the unitary limit is 2.19(35) and roughly confirms ~ 2 as suggested in Ref. [30]. Note that other quantum Monte Carlo calculations in the literature also yield similar values: $\Delta/E_{g.s.} = 2.5(3)$ [28, 29], 2.3(1) [31], and 2.0(2) [27].

TABLE II: $\Delta/E_{g.s.}$ for various values of η

η	Δ/ϵ_F	ξ	$\Delta/E_{g.s.}$
-0.7997	0.172(9)	0.728(37)	0.391(40)
-0.3999	0.271(16)	0.546(34)	0.827(99)
-0.1999	0.326(22)	0.428(30)	1.27(18)
0.0000	0.384(30)	0.292(24)	2.19(35)

V. CRITICAL TEMPERATURE T_c

In the previous two sections, we examined the physical quantities at zero temperature. Thermodynamics at the unitary limit is of much interest [7, 28, 29]. In this section, we examine a representative thermodynamic quantity: the critical temperature of the phase transition, T_c , at the unitary limit.

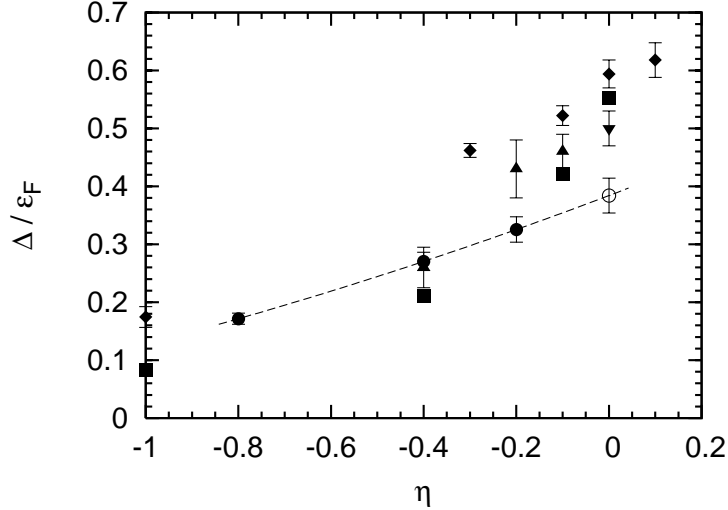


FIG. 5: Pairing gap Δ in the unit of ϵ_F as a function of $\eta \equiv 1/(k_F a_0)$. The solid circles are our Monte Carlo data, shown with statistical uncertainties [1]. The dashed curve is the best fit to the data by use of a quadratic function of η . Δ at the unitary limit $\eta \rightarrow 0$ determined by extrapolation is shown by an open circle. The solid squares, the solid up-triangles, the solid down-triangle, and the solid diamonds are the quantum Monte Carlo data by Bulgac *et al.* [28, 29], by Gezerlis *et al.* [26], by Carlson *et al.* [27], and by Chang *et al.* [31], respectively. Note that the data by Chang *et al.* at $\eta < 0$ are those quoted in Refs. [28, 29].

Figure 6 shows T_c in the thermodynamic and continuum limits for the three values of η by taking from our previous work at the LO [1]. The best fit to the data is also shown in the figure by the dashed curve. It is given by

$$\frac{T_c}{\epsilon_F} = 0.189(12) + 0.149(22) \eta + 0.069(36) \eta^2, \quad (16)$$

which yields the extrapolated value $T_c/\epsilon_F = 0.189(12)$ at $\eta = 0$, or at the unitary limit. For comparison, in the figure we show T_c/ϵ_F by a recent quantum Monte Carlo calculation [29]. While our values are somewhat larger than those of Ref. [29], both show similar η dependence on T_c . This η - T_c dependence is also observed by an ϵ -expansion calculation [41]. Our T_c is tabulated for various values of η in Table III.

In Fig. 7, we summarize various values of T_c at the unitary limit that are reported in the literature, together with ours for comparison. The figure includes the two groups of the T_c determination: by Monte Carlo calculations and by the ϵ -expansion method.

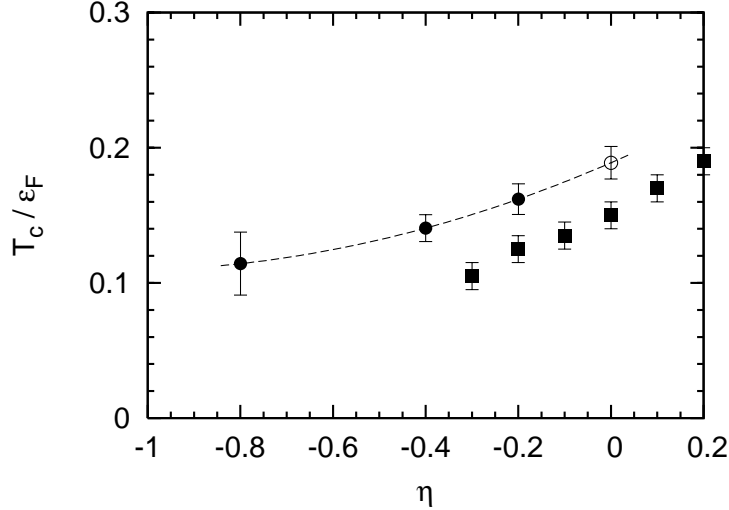


FIG. 6: η dependence of the critical temperature T_c , shown in the unit of ϵ_F . Our Monte Carlo data at the thermodynamic and continuum limits are shown by solid circles, and the extrapolated unitary-limit point is shown by an open circle. The extrapolation is made using the fit function, Eq. (16). For comparison, the solid squares show a recent quantum Monte Carlo result [29].

TABLE III: T_c/ϵ_F for various values of η .

η	T_c/ϵ_F
-0.7997	0.114(23)
-0.3999	0.141(10)
-0.1999	0.162(11)
0.0000	0.189(12)

The Monte Carlo results include $T_c/\epsilon_F = 0.23(2)$ by the determinantal quantum Monte Carlo method on $N_s = 6^3$ and 8^3 lattices [37, 42]; $T_c/\epsilon_F < 0.15(1)$ by the determinantal quantum Monte Carlo method on $N_s = 6^3, 8^3$, and 10^3 lattices [29]; $T_c/\epsilon_F < 0.14$ by the hybrid Monte Carlo method on $N_s = 4^3, 5^3$, and 6^3 lattices [11]; $T_c/\epsilon_F = 0.152(7)$ by a diagrammatic determinantal quantum Monte Carlo method with the finite-size scaling [6]; and $T_c/\epsilon_F \approx 0.25$ by a restricted path integral Monte Carlo method [43].

The ϵ -expansion results [41] include $T_c/\epsilon_F \approx 0.249$ and $T_c/\epsilon_F \approx 0.153$ by up to the NLO

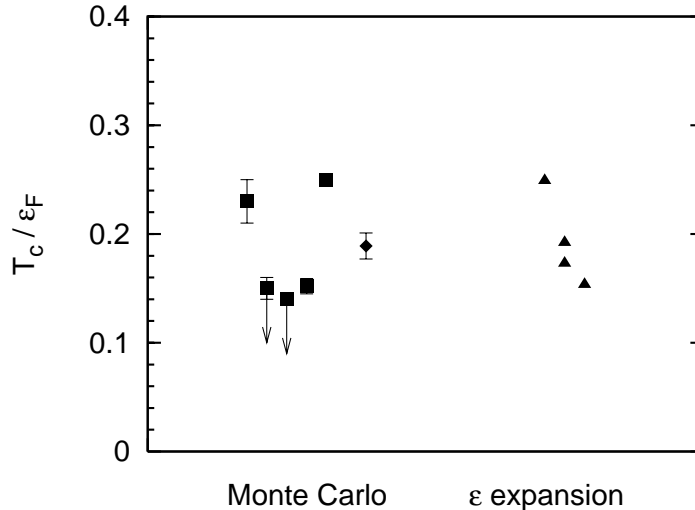


FIG. 7: Critical temperature T_c at the unitary limit appearing in the literature and our extrapolated T_c (all shown in the unit of ϵ_F). The solid squares (with statistical uncertainties) on the left-hand side of the figure are by Monte Carlo calculations [6, 11, 29, 37, 42, 43], and the solid triangles on the right-hand side are by ϵ expansion calculations [41]. Our T_c is shown by the solid diamond with the statistical uncertainty. The horizontal scale is used merely for the separation of each T_c value. The T_c 's by the ϵ expansion calculations are grouped into two in the same way as in Fig. 4. See the text for the reference of each T_c .

in the ϵ expansion about the four and two dimensions, respectively; and $T_c/\epsilon_F = 0.173$ and 0.192 by the Borel-Padé approximation between the four and two dimensions. As noted in the case of the ξ determination, the ϵ expansion seems to indicate a possibly problematic behavior at higher orders [24].

Our T_c at the thermodynamic and continuum limit is also shown in the Monte Carlo group of Fig. 7. Our result $T_c/\epsilon_F \approx 0.189(12)$ seems to be consistent with others, especially with that of Ref. [6], which is the only other T_c obtained in the thermodynamic and continuum limits.

VI. CONCLUSION

We extrapolate our Monte Carlo results for low-density neutron matter [1] to the unitary limit for the following quantities: the ground-state energy $E_{g.s.}$, the pairing gap Δ at $T \approx 0$,

and the critical temperature of the normal-to-superfluid phase transition T_c . All quantities show a smooth extrapolation to the limit in terms of $\eta = 1/(k_F a_0)$. Although no accurate determination of these quantities is yet available, our extrapolated values are in reasonable agreement with those in the literature. Our successful extrapolation suggests that much of the physics of low-density neutron matter [of about $(10^{-4} - 10^{-2})\rho_0$] is similar to the physics of the attractively interacting fermion system at the unitary limit.

ACKNOWLEDGMENTS

We thank M. Ueda for suggesting comparison of our neutron matter calculation to those of the unitary limit and D. Lee for his useful comments after reading the manuscript. We thank R. McKeown for the generous hospitality at Kellogg Radiation Laboratory at Caltech, where a part of the project was carried out. Some of this work was also performed at the Yukawa Institute for Theoretical Physics (YITP), Kyoto University. R. S. thanks the YITP for its warm hospitality. Lattice calculations were carried out on the Seaborg, the Bassi, and the Franklin at the National Energy Research Scientific Computing Center, which is supported by the Office of Science of the U.S. Department of Energy under Contract No. DE-AC03-76SF00098, and at Titech Grid, and TSUBAME, Tokyo Institute of Technology, Japan. This work is being supported by the U.S. Department of Energy under Grant No. DE-FG02-87ER40347 at CSUN.

-
- [1] T. Abe and R. Seki, Phys. Rev. C **79**, 054002 (2009).
- [2] R. Seki, U. van Kolck, and M. J. Savage, *Nuclear Physics with Effective Field Theory; Proceedings of the Joint Caltech/INT Workshop* (World Scientific, Singapore, 1998); P. F. Bedaque, M. J. Savage, R. Seki, and U. van Kolck, *Nuclear Physics with Effective Field Theory II; An INT Workshop* (World Scientific, Singapore, 2000).
- [3] A. J. Leggett, J. Phys. (Paris) **41**, C7–19 (1980); P. Nozieres and S. Schmitt-Rink, J. Low Temp. Phys. **59**, 195 (1985); Q. Chen, J. Stajic, S. Tan, and K. Levin, Phys. Rep. **412**, 1 (2005) and references therein.
- [4] D. M. Brink and R. A. Broglia, *Nuclear Superfluidity; Pairing in Finite Systems* (Cambridge University, Cambridge, England, 2005), and references therein.
- [5] M. Randeria, in *Bose-Einstein Condensation*, edited by A. Griffin, D. Snoke, and S. Stringari (Cambridge University, Cambridge, England, 1994) p. 355.
- [6] E. Burovski, N. Prokof'ev, B. Svistunov, and M. Troyer, Phys. Rev. Lett. **96**, 160402 (2006); New J. Phys. **8**, 153 (2006), and references therein.
- [7] H. Heiselberg, Phys. Rev. A **63**, 043606 (2001); J. R. Engelbrecht, M. Randeria, and C. A. R. Sá de Melo, Phys. Rev. B **55**, 15153 (1997); C. A. R. Sá de Melo, M. Randeria, and J. R. Engelbrecht, Phys. Rev. Lett. **71**, 3202 (1993).
- [8] H. P. Noyes, Annu. Rev. Nucl. Sci. **22**, 465 (1972).
- [9] T. Abe, R. Seki and A. N. Kocharian, Phys. Rev. C **70**, 014315 (2004); **71**, 059902(E) (2005).
- [10] D. Lee, Phys. Rev. B **73**, 115112 (2006).
- [11] D. Lee and T. Schäfer, Phys. Rev. C **73**, 015202 (2006).
- [12] D. Lee, Phys. Rev. C **78**, 024001 (2008).
- [13] D. Lee, arXiv:0804.3501.
- [14] J.-W. Chen and D. B. Kaplan, Phys. Rev. Lett. **92**, 257002 (2004).
- [15] U. van Kolck, Nucl. Phys. **A645**, 273 (1999).
- [16] G. P. Lepage, Lecture at the VIII Jorge André Swieca Summer School, Brazil, 1997; arXiv:nucl-th/9706029.
- [17] R. Seki and U. van Kolck, Phys. Rev. C **73**, 044006 (2006).
- [18] G. N. Watson, Q. J. Math. (Oxford) **10**, 266 (1939); A. A. Maradudin, E. W. Montroll,

- G. H. Weiss, R. Herman, and H. W. Milnes, Acad. R. Belg. Cl. Sci. Mem. Coll. 4^o (2) 14 (1960) No. 7.
- [19] E. Y. Loh Jr. and J. E. Gubernatis, in *Electronic Phase Transitions*, edited by W. Hanke and Yu. V. Kopayev (Elsevier, Amsterdam, 1992).
- [20] R. R. dos Santos, Braz. J. Phys. **33**, 36 (2003).
- [21] H. J. Rothe, *Lattice Gauge Theories: An Introduction*, World Scientific Lecture Notes in Physics, 3rd ed. (World Scientific Pub. Co., 2005); J. Smit, *Introduction to Quantum Fields on a Lattice* (Cambridge Univ. Press, 2002); I. Montvay and G. Münster, *Quantum Fields on a Lattice*, Cambridge Monographs on Mathematical Physics (Cambridge Univ. Press, 1997); M. Creutz, *Quarks, Gluons and Lattices*, Cambridge Monographs on Mathematical Physics (Cambridge Univ. Press, 1985); and references quoted therein.
- [22] D. Lee, Eur. Phys. J. A **35**, 171 (2008).
- [23] J. W. Chen and E. Nakano, Phys. Rev. A **75**, 043620 (2007).
- [24] P. Arnold, J. E. Drut, D. T. Son, Phys. Rev. A **75**, 043605 (2007).
- [25] G. E. Astrakharchik, J. Boronat, J. Casulleras, and S. Giorgini, Phys. Rev. Lett. **93**, 200404 (2004).
- [26] A. Gezerlis, and J. Carlson, Phys. Rev. C **77**, 032801(R) (2008).
- [27] J. Carlson and S. Reddy, Phys. Rev. Lett. **95**, 060401 (2005).
- [28] A. Bulgac, J. E. Drut, P. Magierski, and G. Wlazlowski, arXiv:0801.1504.
- [29] A. Bulgac, J. E. Drut, and P. Magierski, Phys. Rev. A **78**, 023625 (2008).
- [30] J. Carlson, S. Y. Chang, V. R. Pandharipande, and K. E. Schmidt, Phys. Rev. Lett. **91**, 050401 (2003).
- [31] S. Y. Chang, V. R. Pandharipande, J. Carlson, and K. E. Schmidt, Phys. Rev. A **70**, 043602 (2004).
- [32] K. M. O'Hara, S. L. Hemmer, M. E. Gehm, S. R. Granade, and J. E. Thomas, Science **298**, 2179 (2002); M. E. Gehm, S. L. Hemmer, S. R. Granade, K. M. O'Hara, and J. E. Thomas, Phys. Rev. A **68**, 011401(R) (2003).
- [33] T. Bourdel, L. Khaykovich, J. Cubizolles, J. Zhang, F. Chevy, M. Teichmann, L. Tarruell, S. J. J. M. F. Kokkelmans, and C. Salomon, Phys. Rev. Lett. **93**, 050401 (2004).
- [34] M. Bartenstein, A. Altmeyer, S. Riedl, S. Jochim, C. Chin, J. H. Denschlag, and R. Grimm, Phys. Rev. Lett. **92**, 120401 (2004).

- [35] J. Kinast, A. Turlapov, J. E. Thomas, Q. Chen, J. Stajic, and K. Levin, *Science* **307**, 1296 (2005).
- [36] G. B. Partridge, W. Li, R. I. Kamar, Y. Liao, and R. G. Hulet, *Science* **311**, 503 (2006).
- [37] A. Bulgac, J. E. Drut, and P. Magierski, *Phys. Rev. Lett.* **96**, 090404 (2006).
- [38] Y. Nishida and D. T. Son, *Phys. Rev. Lett.* **97**, 050403 (2006).
- [39] Y. Nishida and D. T. Son, *Phys. Rev. A* **75**, 063617 (2007).
- [40] Y. Nishida, *Phys. Rev. A* **79**, 013627 (2009).
- [41] Y. Nishida, *Phys. Rev. A* **75**, 063618 (2007).
- [42] A. Bulgac, J. E. Drut, and P. Magierski, *Phys. Rev. Lett.* **99**, 120401 (2007).
- [43] V. K. Akkineni, D. M. Ceperley, and N. Trivedi, arXiv:cond-mat/0608154.